Naval Research Laboratory

Washington, DC 20375-5320

NRL/MR/6386--92-7179

Assessment of Single-Pulse Laser Damage to Structural Materials for Spacecraft

F.R. STONESIFER

Mechanics of Materials Branch
Materials Science and Technology Division

AND

P.W. RANDLES AND J.A. NEMES

Defense Nuclear Agency
Kirtland Air Force Base, NM

December 24, 1992

REPORT DOCUMENTATION PAGE

Form Approved
OMB No. 0704-0188

1. AGENCY USE ONLY (*Leave Blank*)	2. REPORT DATE	3. REPORT TYPE AND DATES COVERED
	December 24, 1992	

4. TITLE AND SUBTITLE

Assessment of Single-Pulse Laser Damage to Structural Materials for Spacecraft

5. FUNDING NUMBERS

62234N

6. AUTHOR(S)

P.W. Randles,* F.R. Stonesifer and J.A. Nemes*

7. PERFORMING ORGANIZATION NAME(S) and ADDRESS(ES)

Naval Research Laboratory
Washington, DC 20375-5320

8. PERFORMING ORGANIZATION REPORT NUMBER

NRL/MR/6386--92-7179

9. SPONSORING/MONITORING AGENCY NAME(S) AND ADDRESS(ES)

Office of Naval Technology
800 N. Quincy Street
Arlington, VA 22217-4274

10. SPONSORING/MONITORING AGENCY REPORT NUMBER

11. SUPPLEMENTARY NOTES

*Defense Nuclear Agency, Kirtland AFB,
*Consultant (Formerly of NRL)

12a. DISTRIBUTION/AVAILABILITY STATEMENT

Approved for public release, distribution is unlimited.

12b. DISTRIBUTION CODE

13. ABSTRACT (*Maximum 200 words*)

Laser radiation damage to structural or shielding materials can occur by several quite different mechanisms. For continuous-wave and repetitively-pulsed radiation, the damage has been found to be primarily thermal. However, for a single laser pulse of very high intensity and short duration, spalling and mechanical damage become the principal failure mechanism and time does not allow extensive thermal degradation.

In exposure of opaque materials to a high-energy short-duration laser pulse, an expanding plasma is formed on the material surface and a mechanical pulse is transmitted into the remaining target material. This compression wave, attenuated by the target material, reflects off the free or low impedance boundary at the back surface as a tension wave. If conditions are favorable, both front and back faces may spall causing complete penetration of the material. The magnitude of the dynamic stress pulse is dependent on intensity, wave length, and pulse duration as well as the target-material properties and thickness.

A discussion of pressure/impulse, wave attenuation, and spallation is presented. Equations are developed. Experimental data available in the literature, from both flyer-plate and laser shock tests, are plotted and compared for various classes of thin structural materials.

14. SUBJECT TERMS

Laser Damage
Spacecraft Materials
Single-Pulse Shock
Spallation

15. NUMBER OF PAGES

28

16. PRICE CODE

17. SECURITY CLASSIFICATION OF REPORT	18. SECURITY CLASSIFICATION OF THIS PAGE	19. SECURITY CLASSIFICATION OF ABSTRACT	20. LIMITATION OF ABSTRACT
UNCLASSIFIED	UNCLASSIFIED	UNCLASSIFIED	UL

NSN 7540-01-280-5500

Standard Form 298 (Rev. 2-89)
Prescribed by ANSI Std 239-18
298-102

CONTENTS

ASSESSMENT OF SINGLE-PULSE LASER DAMAGE TO STRUCTURAL MATERIALS FOR SPACECRAFT

Introduction

Laser radiation damage to structural or shielding materials can occur by several quite different mechanisms. Material damage from continuous wave (CW) laser radiation has been well documented with experimental as well as analytical results for various classes of structural materials, i.e. see [1].[1] CW radiation damage has been found to be primarily, if not completely, thermal and, for opaque materials, is purely a surface effect. Repetitively pulsed (RP) laser radiation can add additional mechanical damage to the thermal degradation and ablation. Only a limited amount of experimental data exist allowing a direct comparison between CW and RP radiation effects on various structural materials [2]. In both CW and RP damage, time and thermal conductivity are important parameters. For a single laser pulse of very high intensity and short duration, spalling and mechanical damage become the principal failure mechanisms and time does not allow for extensive thermal degradation. Experimental data in this area is sparse. Analytical assessments are typically based on data obtained from other impact methods such as flyer-plate experiments. This report considers only single pulse laser effects on thin structural materials and relies on available pulsed laser as well as flyer-plate experimental data.

Exposure to a high-energy short-duration laser pulse can cause front face and/or back face spallation in structural materials. (Projectile and flyer-plate experiments typically produce back face spallation only.) In opaque materials, a thin layer of material on the front (irradiated) surface is quickly vaporized by the laser energy. An expanding plasma is formed on the material surface and a mechanical pulse is transmitted into the remaining target material. This compression wave, attenuated by the target material, reflects off the free or low impedance boundary at the back surface as a tension wave. In a simplified model, a spall, or spalls, form when the tensile stress in the material exceeds the material's ultimate tensile strength. In partially transparent materials, such as Kevlar/epoxy and s-glass/epoxy, the energy is deposited in a surface layer with a thickness, or depth, dimension. This causes a complex in-depth energy deposition where thermal degradation, pyrolysis and dynamic stress effects can combine to cause front-face spallation failures [3]. If the conditions are favorable both front and back faces may spall causing complete penetration of the material. The magnitude of the dynamic stress pulse is dependent on intensity and pulse duration as well as the target-material properties and thickness.

The energy that actually is absorbed by the target is an important variable. Absorptivity depends on wavelength and intensity of the impending beam as well as the target material and surface condition. Surface coatings that are opaque and non-

[1] Numbers in brackets refer to references at end of text.

Manuscript approved November 23, 1992.

reflective to the impending wavelength will increase the energy absorbed and greatly influence the spall threshold [4]. A coating of flat black paint (dispersion of carbon black particles in acrylic resin) can increase the peak pressure by about one order of magnitude over that for uncoated samples for pulses in the 100 J/cm^2 fluence range [5]. A target coating that is transparent to the incoming laser wavelength can confine the plasma at the material surface and may decrease the laser energy spall threshold (increase the effective shock wave) by nearly an order of magnitude [6]. Such considerations may be important for spacecraft where protective or thermal coatings are normally applied to the structures without thought of possible effects on laser survivability.

Approach

Some of the many variables associated with this problem have been mentioned previously. We will first attempt to establish a relationship between the laser's intensity, or fluence, and an equivalent pressure pulse to the specimen. This relationship is highly dependent on the target material and surface condition as well as the intensity, wavelength, and pulse length of the laser radiation. Surface pressure pulses are usually measured experimentally and an empirical relationship established as a function of intensity, or fluence, raised to a power.

The next consideration is the attenuation of the shock wave within the target material. This is highly dependent on the target material and thickness as well as the pressure pulse-length. The purpose here is to establish simple formulas for estimating the attenuation of short duration shock waves in structural and shielding materials. Two main forms of attenuation predominate and are treated here. First is the hydrodynamic attenuation present in all materials at sufficiently high stress levels. This attenuation is due to the fact that nearly all materials release from a compressive shocked state with a faster velocity than the shock velocity which lead to that state. Hence, for any pulse shape, of finite duration, the release finally overruns the original shock. This is especially true for very short and intense shock pulses. The second form of attenuation is due to dispersive effects in heterogeneous materials. Dispersive attenuation is present at all stress levels, even linearly elastic, for finite duration stress waves and it is caused by the multiple scattering and spreading of the pulse. Hydrodynamic attenuation is most important for very short and intense shock pulses, while dispersive attenuation is most important for large impedance mismatches and large structural scales in heterogeneous materials. In many cases, both effects are present and the approach taken here is to assume that a product relationship of the two effects taken separately will be adequate to estimate the combined effects.

Damage (spallation is of most interest here) results from the reflection of the attenuated shock pulse at a free or low impedance back face with subsequent tensile failure or degradation. This presents the very difficult problem of trying to establish fairly simple screening models for assessing the spall toughness of materials. Physical damage is the end result in a series of complicated processes consisting of shock wave initiation at the front face, propagation and attenuation of the shock pulse

through the material, and reversal or release at the back face to place the material in a fleeting tension state. Thus, damage is the cumulation of a series of processes each with its uncertainties. In addition the damage itself is a highly time-dependent and complex process. Accuracy and justice can probably be done to this subject only by detailed and specific tests and observations with predictive models possible only if careful account is taken of important effects, the evolutionary behavior of the damage processes, and correlation with the experimental evidence. Such an approach is far beyond the scope of the present task. Thus, a simple time at stress above a threshold criterion will be used here. This will not allow for the evolutionary behavior of damage and will not include the important softening effects of damage on subsequent response. However, it will include the observed toughening of real materials to high tensile stresses for very short durations and it will relate damage to impulse (above a threshold) delivered to the material.

When these two relationships, surface-pressure vs. intensity and attenuation vs. material, are established, one can then attempt to model the conditions for spall threshold, for a given material and laser beam, in terms of target thickness and beam intensity.

As stated earlier, experimental data in this area are sparse and large gaps exist in the available data. More experimental data have been published on aluminum foil than on any other material. Therefore, we shall consider aluminum first and then extrapolate to include what data there are available for other structural materials of interest to spacecraft engineers. We will use aluminum as a basis for comparison for other materials. Most of the available experimental single-pulse laser data were obtained using a neodymium-glass (Ne:glass) laser which produces a 1.06 micron (μm) wavelength. Pulse durations at 1/2 maximum vary over the range of 0.5 to 30 nanoseconds (ns).

Pressure/Impulse

Mc Kay and Laufer [7] have published a compilation of laser-produced impulse and pressure generation data. They compiled data for various wave lengths in air, vacuum, and reduced air. These data are for longer pulse lengths and lower intensities than is usually required for spallation of structural materials and no mention is made in the report of mechanical damage to the target material. Their plots are nearly all for irradiances below 10^{11} W/cm^2. Our interest is more in the range of 10^{11} W/cm^2 and above, however, they do present some elementary models that probably can be extended into our range of interest. Problems arise in comparing the experimental data from various experimenters. Some experimenters measured pressure while others measured impulse. Impulse generation in air is quite different than in a vacuum. When comparing data we have to be sure we fully understand what parameters are being measured, in what medium the experiments were performed, and what units of measure are recorded.

To determine the peak surface pressure, which would equal the stress within the target surface, Mc Kay and Laufer [7] suggest what they call the "Pirri/Raizer" model. This can be expressed as:

$$p_s = 684 \times \rho^{1/3} I^{2/3} \quad [2] \quad (1)$$

where p_s is the surface pressure in dynes/cm^2, ρ is the density of the medium in g/cm^3 (1.22×10^{-3} for air at sea level) and I is the irradiance in W/cm^2. Determining the impulse in air is much more complicated and requires a "modest computer program". They recommend the "Simons model" [8] which defines eight distinct regimes based on various combinations of laser and target parameters. Impulse coupling coefficients are calculated from plots generated with the model.

Determining equivalent surface pressure and impulse for given laser pulses in a vacuum is much more straight forward. Reference [7] suggests the "Pirri expression" which can be written as:

$$p_s = 0.0425 (M^{7/2} C^2 I^7 / r_s \lambda^2)^{1/9} \quad (2)$$

where:

p_s = peak surface pressure in d/cm^2,
M = atomic weight of the target material, amu,
C = speed of light,
λ = Laser wavelength, in units consistent with C,
r_s = spot radius, cm, and
I = laser irradiance, W/cm^2.

The impulse coupling coefficient, I/E (dyne-sec/joule), can be obtained by dividing the pressure by the irradiance, (p_s/I), which, using equation (2), gives:

$$I/E = 0.0425 (M^{7/2} C^2 / I^2 r_s \lambda^2)^{1/9}. \quad (3)$$

Beverly and Walters [9] also use the Pirri [10] and Raizer [11] theories to develop the relationship,

$$p_s = 6.43 \times 10^{-3} \rho_o^{1/3} I^{2/3}, \quad (4)$$

where surface pressure, p_s, is in bars and the other parameters are as stated above for equation (1). They show that their results agree very well with those obtained by Edwards, et al.[12] using the LASNEX code.

It may help the reader later in this report to be reminded that:

10^6 dyne/cm^2 = 1 bar = 10^5 pascal, therefore,
1 Kbar = 10^9 d/cm^2 = 10^8 Pa = 10^{-1} GPa..

[2]The density in Eq. (1) has been normalized to sea level.

Attenuation

Hydrodynamic Attenuation

Hydrodynamic attenuation is due to nonlinearities in the compaction behavior which leads to increasing resistance to the shocked state as compression or volume reduction increases. Hence the effective bulk modulus and shock velocity increase with increasing shock pressure. However, since the release is on the shocked isentrope, it is at an even higher effective modulus and the release wave overruns the shock and attenuates it. There are two asymptotes to this general behavior. First, on the low stress or pressure end, which occurs after sufficient propagation, any pulse becomes entirely elastic and no further attenuation occurs. The other asymptote is at vanishing duration, infinite magnitude. This condition is approached at the front face under extreme conditions, but, in general, can be thought of as occurring in front of the front face. These asymptotes are illustrated in Figure 1 with the front face at $x=x_0$.

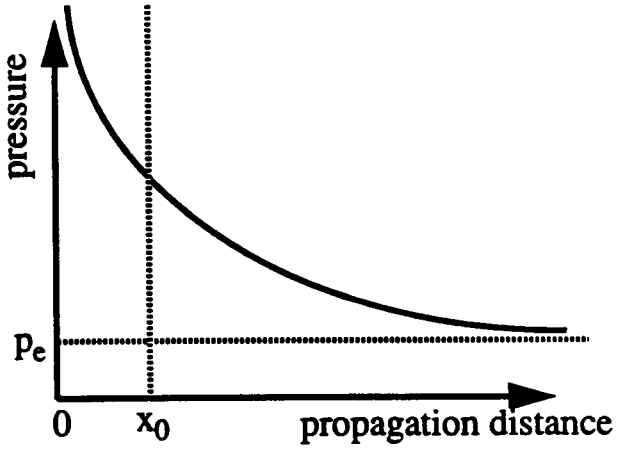

Figure 1. Asymptotic Behavior of Hydrodynamic Attenuation.

This form of attenuation is described adequately by a hyperbolic power law ,

$$p(x) = p_e + \beta(x/L_h)^{-\alpha} \quad , \qquad (5)$$

where p_e and $x=0$ are the asymptotes in Figure I. A normalization length is introduced to account for pulse length and amplitude. It is given by $L_h = I_o/z = c_o t_o p_o/(\rho c_o^2)$ where $I_o = p_o t_o$ is the impulse delivered to the target material (triangular pulse shape assumed), $z = \rho c_o$ is the acoustical impedance, p_o is the front face pressure, t_o is the half-maximum front face pulse duration, c_o is the acoustical propagation velocity, and ρ is the material density. A material constant governing attenuation is given by α, and β is related to the front face pressure by Equation (5) as $p_o \equiv p(x_o) = p_e+\beta(x_o/L_h)^{-\alpha}$.

With this, Equation (5) can be rewritten as

$$p(x) = p_e + [p_o - p_e] (x/x_o)^{-\alpha}. \quad (6)$$

This power law description is a general approximate representation for hydrodynamic attenuation which allows the front face to be shifted to $x = x_o$ to match the front face pressure p_o. The rate of attenuation is then controlled by the material parameter α and the normalized propagation distance x/L_h or x/x_o. The normalized length L_h or the propagation distance x_o (from an idealized delta function pulse at $x = 0$ to the actual pulse shape and magnitude at $x = x_o$) enter to normalize the length scale and account for pulse-length and magnitude effects. In the following, this description is found to adequately describe attenuation of short pulses in aluminum and, for lack of sufficient data, will be used for the hydrodynamic attenuation for all materials considered here.

Dispersive Attenuation

Composites and other heterogeneous materials exhibit another type of attenuation due to multiple scattering or dispersal of waves. This is called dispersive attenuation and it, like hydrodynamic attenuation, is especially pronounced for very short pulses. Unlike hydrodynamic attenuation, dispersion is present even for vanishingly small amplitude waves. Dispersive attenuation is derivable from Christensen's work [13], and decays as

$$p(x) \sim p_o[x_p^3/(L^2 x)]^{1/3}. \quad (7)$$

The half-max-pulse length is $x_p = c_o t_o$ and p_o is the front face pressure. A measure of the dominant heterogeneous length scale (such as laminate period for a laminated composite) is denoted by L. Equation (6) is only an indication of asymptotic behavior for large propagation distances x and, thus, does not give $p(0) = p_o$. The dispersive attenuation behavior expected is shown in Figure 2. This general behavior applies for any triangular shaped pulse that is peaked at pressure p_o at $x = 0$ and begins to attenuate immediately as the pulse propagates into the material. A laser pressure pulse tends to conform to this shape. A flat top pulse with a dwell at constant pressure would not attenuate until the dispersion affecting the loading and unloading portions of the pulse begin to interact. Then the attenuation would follow the form given by Equation (7) and shown in Figure 2.

Combined Attenuation

These two attenuation mechanisms can be combined in a somewhat heuristic manner by assuming dispersion and hydrodynamic effects do not strongly interact so

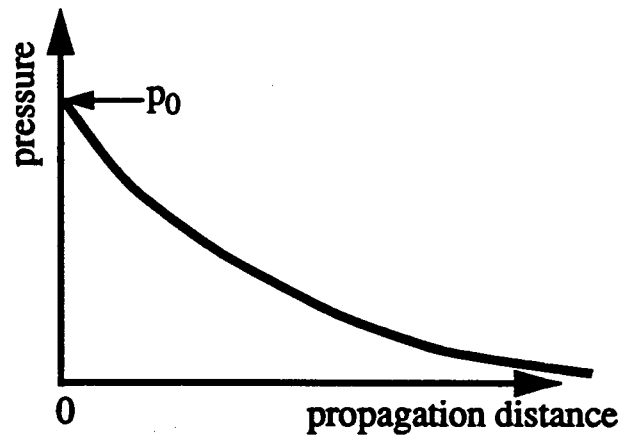

Figure 2. Dispersive Attenuation.

that their combined effects are multiplied as follows:

$$\begin{bmatrix}\text{Combined}\\ \text{Attenuation}\end{bmatrix} = \begin{bmatrix}\text{Attenuation due to}\\ \text{Dispersion alone}\end{bmatrix} \times \begin{bmatrix}\text{Attenuation due to}\\ \text{Hydrodynamic effects}\\ \text{alone}\end{bmatrix}. \quad (8)$$

In order to do this combination, Equations (5) and (7) must be centered at x=0, so that the front face is the same for each effect, and the normalizations for propagation distance x must be made more specific. Following from Equations (5) and (7), Equation (8) can be written as

$$p(x) = [1 + C_d(L^2 x/x_p^3)]^{-1/3}\ [p_e + \beta(\gamma + x/L_h)^{-\alpha}]\ . \quad (9)$$

C_d is a dimensionless dispersive scaling parameter and γ is a hydrodynamic shift parameter to properly center both effects at x = 0. The form (9) is seen to have the following desirable properties: 1) $p(0) = p_e + \beta\gamma^{-\alpha} \equiv p_0$, 2) as $x_p \to \infty$(long pulse limit), $p(x) \to p_0$, 3) as $x_p \to 0$ (short pulse limit), $p(x) \to 0$, 4) as $L \to 0$ (homogeneous limit), $p(x) \to$ pure hydrodynamic attenuation, and 5) as $p_0 \to p_e$ (elastic limit), $p(x) \to$ pure dispersive attenuation. The general behavior given by Equation (9) is shown in Figure 3.

The parameters γ and C_d in (9) just introduce added difficulty in establishing the combined attenuation. Certainly, γ can be obtained only by fitting experimental data or matching hydrocode computer calculations. The dispersive parameter C_d can be specified for some simple situations, which gives some indication of its general form. For example, in the case of a periodic, two-phase, linearly elastic laminate with one-dimensional wave propagation in a direction normal to the lamina, C_d takes the form

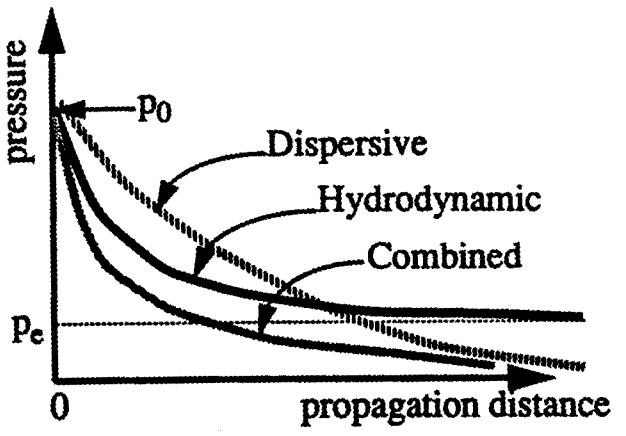

Figure 3. Combined Hydrodynamic and Dispersive Attenuation.

$$C_d \cong 0.814\,(c_o^4\, v_1^2\, v_2^2)/(c_1^2\, c_2^2)\,[(z_1^2 - z_2^2)/(z_1 z_2)]^2 \qquad (10)$$

where c_o is the effective composite propagation velocity and c_n are the velocities, v_n the volume fractions, and z_n the acoustic impedances, respectively, of the individual lamina n =1 and 2. Equation (10), is derivable from Christensen's development for a laminate in [13]. In equation (9), L is the period of the laminate for this case. In general, something like ultrasonic characterization would be required to establish the dispersion parameters for a composite material. This would essentially establish the length scale, $(C_d\, L^2)^{1/2}$, occurring in Equation (9).

Hydrodynamic Attenuation Curve Fitting

Some particular cases, where attenuation data is available, are used to show the validity of the curve forms (5) and (9) and to determine parameters for aluminum. This is by no means comprehensive and leaves the task of fitting parameters to each individual material of interest; however, it will show the general trends and will demonstrate the approach to determining attenuation parameters.

The first case is for general (nondescript) nonlinear material which exhibits very pronounced hydrodynamic attenuation and also shows dependence on pulse length and on front face pressure magnitude. Herrmann [14] has a very nice discussion of hydrodynamic attenuation and includes hydrocode calculations over a range of front face pressures. These results are seen in Figure 22, page 173 of [14] and that data is reproduced and fit with Equation (9) in Figure 4.

Equation (9), with L = 0 for pure hydrodynamic attenuation, was fit to this data by a least squares approach to determine the following parameters: p_e = 0.74 Kb, β = 2149 Kb, α = 0.7063, and the different shift parameters for each p_o are; γ = 208 for p_o = 50 Kb, γ = 25 for p_o = 250 Kb, and γ = 2.9 for p_o = 1000 Kb. The propagation

distance was already normalized with respect to pulse length, c_0t_0, by Herrmann, and that generality is taken into account, but Figure 4 also demonstrates a generality with respect to front face pressure over a range of 50 -1000 Kb for the same attenuation parameters, α and β, and elastic pressure, p_e.

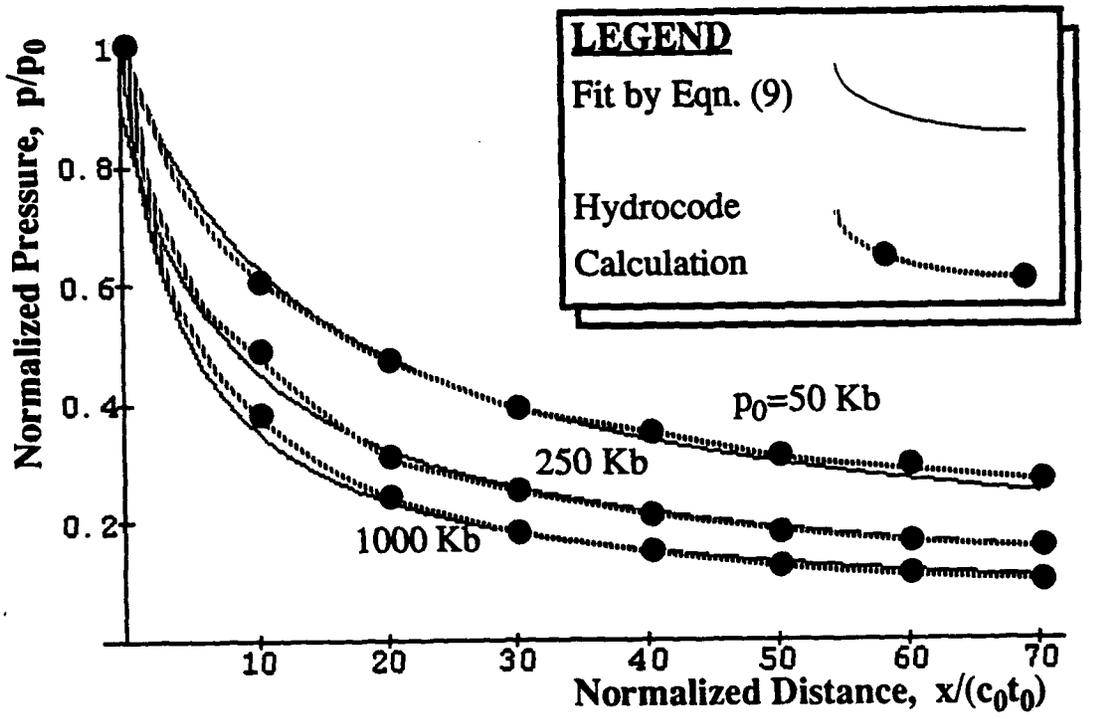

Figure 4. Hydrodynamic Attenuation Curve Fit to Data from [14].

The next case is for aluminum subjected to a short duration laser pulse. An equation of state is used for aluminum and a hydrocode calculation predicts attenuation as a function of propagation distance. This work was done by Eliezer, Gilath and Bar-Noy [15] and is reproduced in Figure 5.

This data is for a 3.9 nanosec laser pulse delivering 9 $x10^{11}$ Watts/cm^2 peak power at wavelength 1.06 μm. The parameters required for the aluminum target are; density ρ = 2.75 gm/cm^3, acoustic velocity c_0 = 5.33 mm/μsec. The estimated front face pressure is 550 Kb with pulse length $x_p = c_0\ t_0$ = 20.8 μm. This gives a normalization length $L_h = c_0\ t_0/(2\rho c_0^2)$ = 7.32 μm. The parameters for the least squares curve fit are p_e = 2.4 Kb (may be related to the yield point and is slightly above the static tensile strength), shift parameter γ = 53.7, β = 1.26 Mb, and attenuation power α = 1.943.

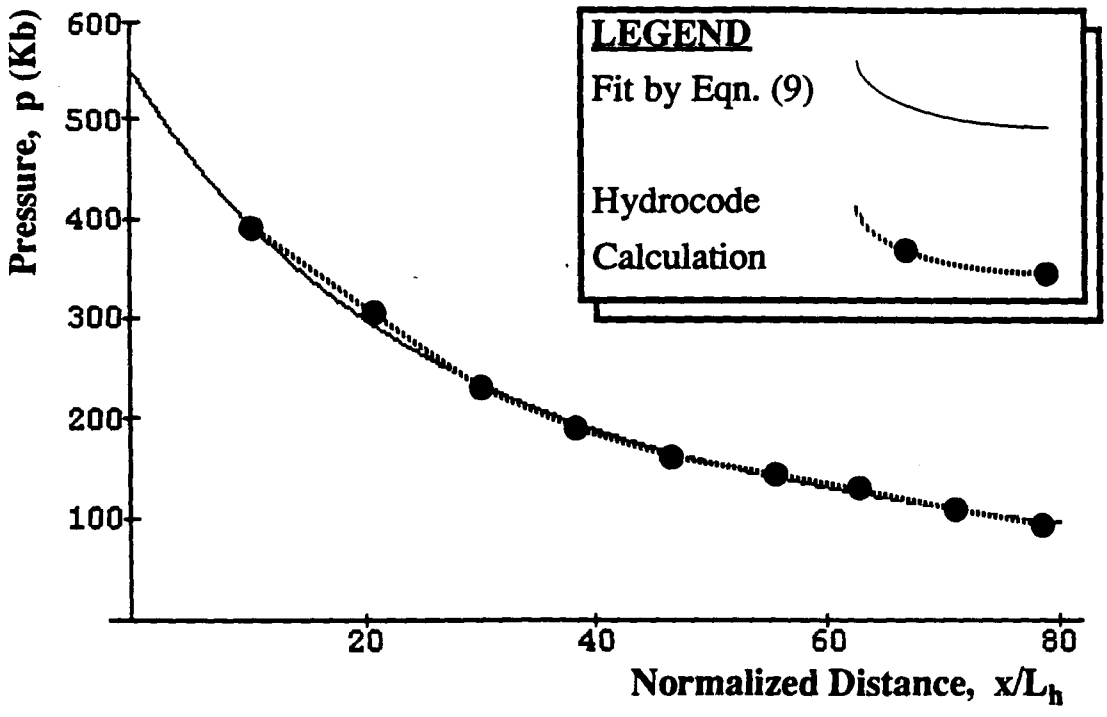

Figure 5. Hydrodynamic Attenuation Curve Fit to Data from [15].

Another example of attenuation in aluminum is taken from Cottet and Boustie [16]. This case is for a very short, 0.6 nanosec, laser pulse, also of wavelength 1.06 μm, delivering a peak intensity of approximately 10^{12} W/cm^2 to the front face. This produces a maximum pressure of about p_o = 830 Kb. These results are from a

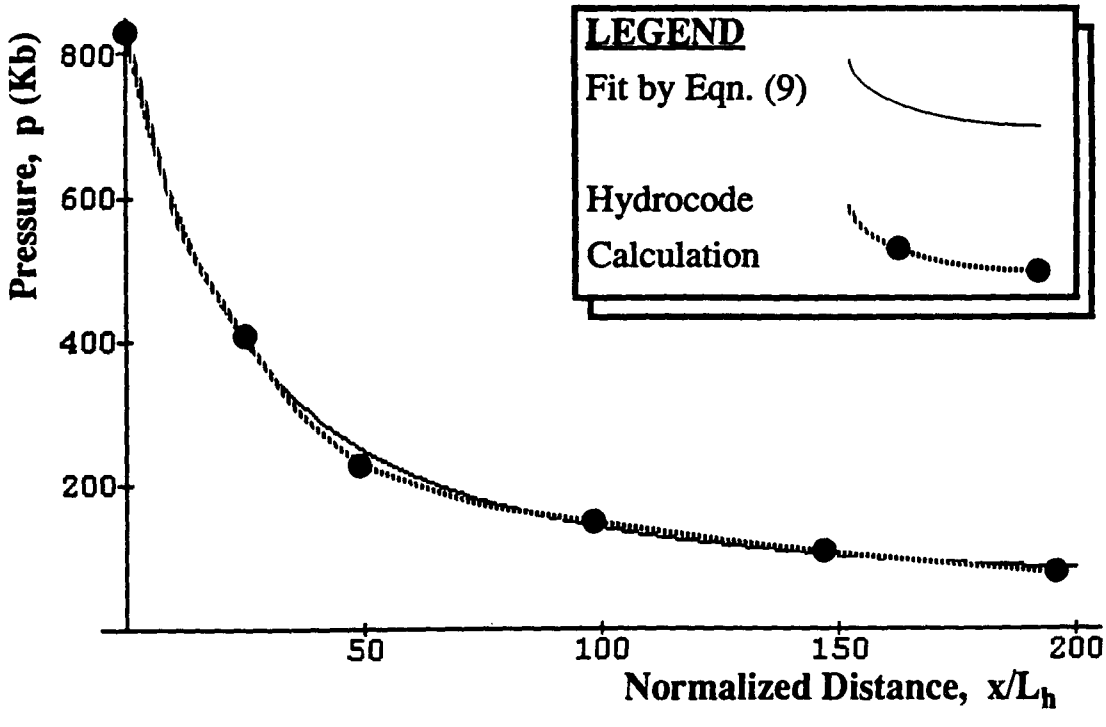

Figure 6. Hydrodynamic Attenuation Curve Fit to Data from [16].

hydrocode calculation using an aluminum equation of state. The data from [16] and the least squares fit using Equation (9) are shown in Figure 6.

The least squares parameters required for this fit follow: $L_h = c_o t_o/(2\rho c_o^2) = 2.04$ μm, $p_e = 51$ Kb (very high and would indicate no hydrodynamic attenuation below this value), shift parameter $\gamma = 47.6$, $\beta = 1.37$ Mb, and attenuation power $\alpha = 1.933$.

Comparing these two examples for aluminum, the parameters for the curve fit by Equation (9) with L = 0 are remarkably similar. The main discrepancy is in the elastic asymptotic pressure, p_e. Since this hydrodynamic attenuation is caused by nonlinearity in the material Hugoniot, p_e could be interpreted as the pressure at which deviation from linearity is detected. In which case, p_e = 2.4 Kb, from the first example. The attenuation parameters can be taken approximately as β = 1.3 Mb and α =2. The normalization length, $L_h = I_o/z$, and the shift parameter, $\gamma = [\beta/(p_o - p_e)]^{1/\alpha}$, are particular to each situation.

Spallation

Spallation is quite complex since it involves a very rapid fracture phenomenon and is the end result, in this application, of several complex processes. These include laser material interaction, pressure application at the front face of the target, propagation and attenuation of the compressive pressure stress wave in the target material, reflection and reversal to a tensile stress wave at the free back face, and finally possible degradation or failure of the material under a very transient tensile stress field. A moderately simple view of spallation will be taken here to remain consistent will the level of approximations which are used in the proceeding processes. Account will be taken of time at stress so that the well-known increase in spall strength with shortening of duration will be present.

A schematic of the reflection and reversal to tension at a free back face is shown in Figure 7.

The tensile reflection is actually subsequent to the arrival of the compressive pulse at the back face, but they are both shown in Figure 7 to illustrate that the pulse shapes are essentially the same once they clear a zone of interference. Thus, the magnitude of the tensile pulse p(H) at the back face x = H will be used from the attenuation estimates, such as Equation (9), to estimate the maximum tensile stress near the back face. This is stated as follows:

$$\sigma_{max} \cong p(H) \qquad (11)$$

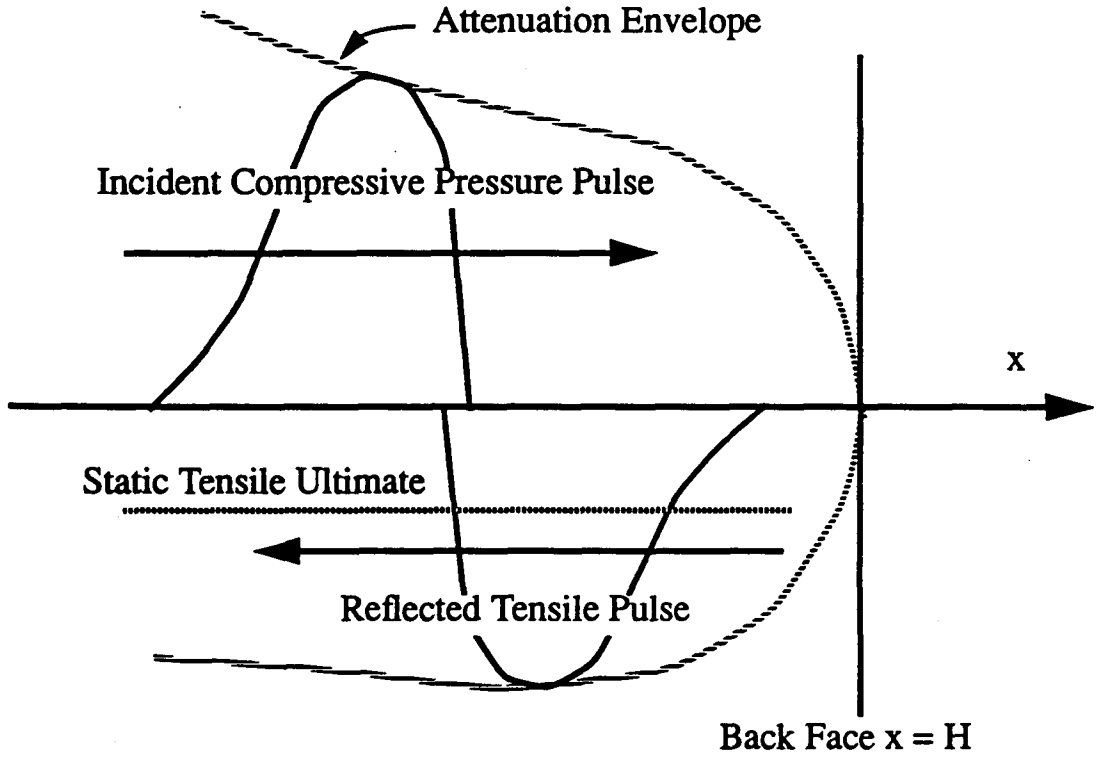

Figure 7. Reversal to Tension at the Back Face.

Further, with linear momentum conserved in the incident compressive pulse,

$$I_o = p_o t_o = p(x)t(x) = p(H)t(H) = \text{constant} \qquad (12)$$

where p_o and t_o are the front face pressure and half-maximum pulse duration, respectively, and p(x) and t(x) are their values at a propagation distance, x. This assumes an approximate triangular pulse shape is maintained from initiation through complete propagation of the material thickness. This is not precisely true, but the approximation is in keeping with the general level of treatment contained in this document. This development is aimed at a time at stress spallation criterion, which follows.

It is hypothesized that the integrated stress above static ultimate with respect to dwell time is a measure of spallation toughness. This sort of dynamic fracture criterion was first proposed by Tuler and Butcher [17] in 1968. In the absence of detailed damage modeling, this is probably the appropriate level of sophistication for the present application. This measure of critical fracture toughness is then just a fraction of the momentum delivered to the back face by the incident compressive pulse as follows:

$$I' = \int^{t} \text{Max}\,[0, \sigma(x,t) - \sigma_{ult}]\,dt \qquad (13)$$

where $\text{Max}[\sigma(x,t)] = \sigma_{max} = p(H)$ is used for x near H, and σ_{ult} is the static ultimate tensile strength. Taking account of the fact that a triangular pulse shape is assumed and that p(H) and t(H) are related by Equation (12); Equation (13), when $I' \geq 0$, can be written explicitly as

$$I' = t(H)\,\frac{[p(H) - \sigma_{ult}]^2}{p(H)} = p_0 t_0 \left[\frac{p(H) - \sigma_{ult}}{p(H)}\right]^2 . \qquad (14)$$

The spallation criterion is then stated as follows: spallation failure occurs if

$$p(H) > \sigma_{ult} \text{ and } I' \geq I'_{ult} \qquad (15)$$

where I'_{ult} must be empirically determined through dynamic fracture tests. Combining Equations (14) and (15), it is seen that the critical back face stress for spallation is a function only of the incident momentum $I_0 = p_0 t_0$ and the ultimate values σ_{ult} and I'_{ult}. This critical spallation pressure is given by

$$p(H) \geq \sigma_{ult} \Big/ \left(1 - \sqrt{\frac{I'_{ult}}{I_0}}\right) \qquad (16)$$

and this dependence is illustrated in Figure 8.

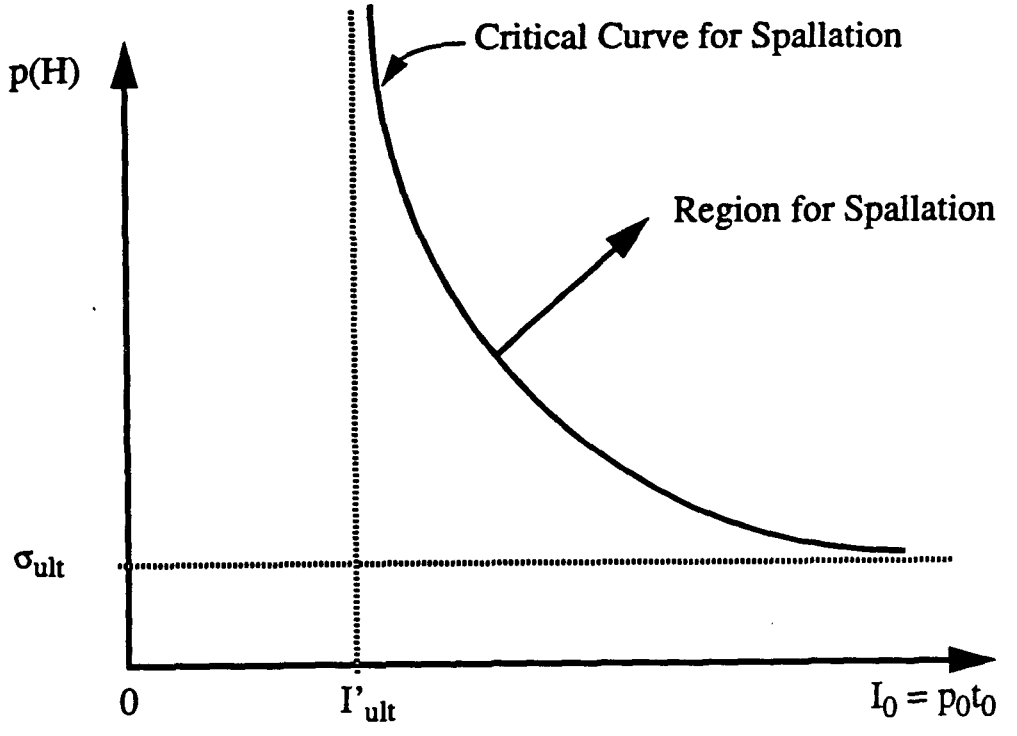

Figure 8. Critical Back Face Pressure Versus Front Face Impulse for Spallation.

This criterion clearly shows strength dominated behavior for long pulse durations (t_0 large) and impulse dominated behavior for short duration pulses. This is qualitatively correct, but would surely require refinement in presence of real data on specific materials or for design requirements to withstand impact or pulsed laser effects. In order to connect spallation with the attenuation material effects which, along with spallation toughness, are the material parameters that can mitigate shock damage, these results must be combined with the estimates on attenuation. That is done in the following section.

Combined Effects of Attenuation and Spallation

The attenuation Equation (9) can now be combined with the spallation Equation (16) to connect front face pressure, p_0, and pulse duration, t_0, with the target thickness, H, and the material parameters. For simplicity, this is done only for the homogeneous case, L = 0, where all attenuation is hydrodynamic. In which case, from Equations (9) and (16),

$$p(H) = p_e + \beta\left(\gamma + \frac{H}{L_h}\right)^{-\alpha} \geq \sigma_{ult}\Big/\left(1 - \sqrt{\frac{I'_{ult}}{I_0}}\right). \qquad (17)$$

Equation (17) can be solved for a p_0 versus H spallation condition using $L_h = I_0/z$ and $\gamma = [\beta(p_0 - p_e)]^{1/\alpha}$ as follows:

$$H \leq \frac{I'_{ult}}{z\delta^2}\left\{\left[\frac{\beta}{\sigma_{ult}/(1-\delta) - p_e}\right]^{1/\alpha} - \left[\frac{\beta}{p_0 - p_e}\right]^{1/\alpha}\right\} \qquad (18)$$

where $\delta = (I'_{ult}/I_0)^{1/2}$, $I_0 = p_0 t_0$, and $z = \rho c_0$ is the acoustic impedance. The general trend of Equation (18) is indicated in Figure 9.

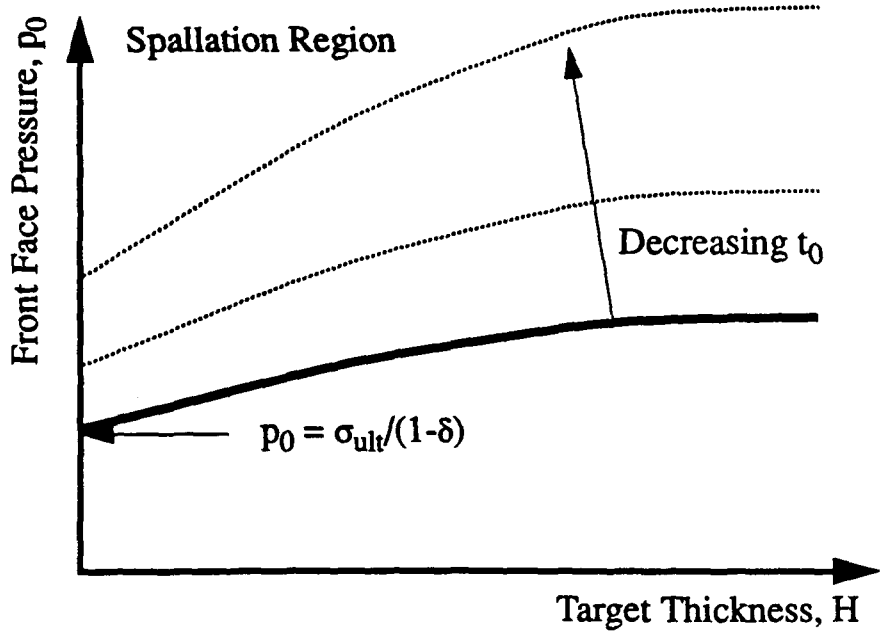

Figure 9. Critical Front Face Impulse Versus Target Thickness for Spallation.

This figure just indicates general trends without an attempt to plot for a specific material. Material parameters required are I'_{ult}, σ_{ult}, α, β, and p_e.

Experimental Data

Aluminum

Cottet and Boustie [18] give a relationship between laser intensity and front-face pressure which works very well for their data on aluminum exposed to single-pulse laser radiation at 1.06 μm wavelength. They used intensities between 5×10^{11} and 5×10^{12} W/cm^2 with pulse duration, at 1/2 max., from 0.5 to 25 ns. Their relationship is given as;

$$p_{max}\ (\text{GPa}) = 12\,[\,I_a\ (\text{W/cm}^2) / 10^{11}\,]^{2/3}, \qquad (19)$$

where p_{max} is the maximum pressure applied *at the surface* of the target and I_a is the *absorbed* intensity. The authors state that, for aluminum, the absorbed intensity is approximately 80% of the incident intensity . (Note the intensity to the 2/3 power as predicted by the model in equation (1).)

In the text of this paper [18] a spallation pressure threshold of about 50 GPa is given for 100 and 250-μm thick pure aluminum foils using a 0.5-ns pulse. Similarly, thresholds are given as 50 GPa for 750-μm and 100 GPa for 1-mm thick foils using a 2-ns pulse. Table 1 shows threshold pressures and corresponding target thicknesses from Figures 1 and 2 [18] listed along with the equivalent laser intensities as calculated from equation (19) given above. This equation gives absorbed intensity, which the authors say was 80% of the incident, therefore the calculated values in the table have been increased by 20%. The data for 3.9 ns pulses were taken from Table II in Eliezer, Gilath, and Bar-Noy [15]. They used a Ne:glass laser and Aluminum foil but it is not clear whether the quoted intensities are equivalent absorbed or measured incident. However, since they measured intensity, not pressure, we can assume that they measured the incident intensity. (Values of intensity, or irradiance (W/cm^2), can be converted to energy values, or fluence (J/cm^2), by multiplying by the pulse width (sec)).

The data listed in Table 1 are shown plotted in Figure 10. Also contained in Figure 10 are correlations with the formulas developed in this document and the material properties and attenuation parameters found for aluminum. These correlations are made using Equation (2) relating front surface pressure to laser intensity in a vacuum for aluminum atomic weight, 1.06-μm wavelength, and 1.5-mm laser spot radius, to get

$$p_s \cong 3.075 \times 10^{-7} \times I^{7/9} \qquad (20)$$

with p_s having units of kilobars and laser intensity, I, having units of Watts/cm^2. This

expression is then inserted into Equation (18) for $p_o = p_s$ so that target thickness, H, is related to laser intensity, I. The correlation curves in Figure 10 are for the threshold equality taken in Equation (18) and for the following properties of aluminum: attenuation exponent, α = 2, β = 1.3 Mb, elastic asymptote, p_e = 2.4 Kb, static ultimate tensile strength, σ_{ult} = 2 Kb, acoustic impedance,z = 14391 Kb-μsec/cm, and ultimate impulse for dynamic fracture, I'_{ult} = 0.4 Kb-μsec (Ktap) (this quantity was adjusted for a "best" fit to the data in Figure 10). The duration of the pressure pulse is thought to be somewhat longer than the laser pulse duration, especially for these nanosecond pulses. However, no information was found on this subject, and the following relationship was used:

(pressure pulse duration) = 10 x (laser pulse duration).

The actual relationship probably depends on the target material and the durations become approximately equal for pulses in the microsecond range.

Table 1: Spallation Thresholds for Aluminum Foil

Pulse width (ns)	Target thickness (μm)	Front surface pressure (GPa)	Equiv. laser intensity (W/cm^2)
	100 and 250	75	1.87×10^{12}
0.5	500	140	4.78×10^{12}
	750	160	5.84×10^{12}
	1000	190	7.56×10^{12}
	100	40	7.31×10^{11}
2	400	35	5.98×10^{11}
	500	45	8.71×10^{11}
	1000	90	2.46×10^{12}
	100	--	7.20×10^{10}
3.9	180	--	1.06×10^{11}
	280	--	1.56×10^{11}
	600	--	2.91×10^{11}

Copper

Eliezer, Gilath, and Bar-Noy [15] report results for copper foil (in addition to the aluminum data) at a pulse width of 3.9 ns. The data on copper are presented here for comparison and to illustrate material property effects. Copper has less attenuation but still requires a higher energy input for spalling than aluminum. Copper threshold data from [15] are listed in Table 2 and shown plotted in Figure 11 along with some carbon/carbon data and an aluminum curve (from Fig.10) for comparison.

Table 2: Spallation Thresholds for Copper Foil

Pulse width (ns)	Target thickness (μm)	Laser intensity (W/cm^2)
3.9	100	1.09×10^{11}
	250	1.85×10^{11}
	400	3.50×10^{11}
	650	5.20×10^{11}

Carbon/Carbon

Gilath, Eliezer, and Weisshaus [19] tested several carbon/carbon materials that were manufactured by different processes. The materials were 0.55 mm thick and irradiated with pulse lengths between 3 and 7.5 ns. Spall thresholds for the materials were between 1.9 and 5.5×10^{10} W/cm^2 depending on the specific material being tested and radiation pulse-length. Walters and Newaz [5] found that for a pure carbon surface, tested in a vacuum with a 30-ns pulse, the peak temperature ($K \times 10^3$) shows a power dependence of 0.48 on pulse fluence (J/cm^2)and noted very strong shock attenuation in the material. They found that the peak pressure (Kb) shows a power dependence of 1.18 on pulse fluence. This band of carbon/carbon data, from [19], is shown plotted in Figure 11 for comparison with the copper and aluminum.

Graphite/Epoxy

Laminated graphite/epoxy composite has very high dispersive shock-wave attenuation properties, but since its transverse tensile strength is low, it still has a relatively low spall threshold. Experimental data from Walters and Clauer [20] indicate that a front surface peak pressure of about 35 Kb is reduced to about 8 Kb after

traveling through a graphite/epoxy laminated specimen only 1.5 mm thick.[3] Walters, et. al. [4] calculated, from experimental data, that the shock speed was 3.33 x 10^5 cm/s for this material. They determined [4] that temperature rises in the material as a 1/2 power of fluence and therefore suggest that the pressure should also rise as the 1/2 power of fluence. In a later report, Walters and Newaz [5] plot experimental data showing peak temperature (K x 10^3) in carbon/polymer rising as the 0.45 power of fluence (J/cm^2), thus confirming the earlier data. However, another plot in the same report shows peak pressure (Kb) rising as a 1.37 power of fluence, rather than the 1/2 power as had been predicted earlier, [4]. They also report that at fluences above 200 J/cm^2 internal cracks develop which "could lead to significant reductions in stiffness and fatigue life." This data is for a 30-ns pulse in a vacuum and was recorded in terms of surface pressure not laser intensity.

Walters, et al. ([4] page 77) concluded, "Significant modulus reductions (>10 percent) occur in 1.5 mm thick uniaxial and angle-ply carbon/epoxy laminates exposed to fluences greater than 200 J/cm^2." This conclusion is important here since spacecraft structures are often designed specifically for stiffness. Another conclusion from this report ([4] page 77) is, "The threshold for internal cracking near the rear surface of 3.0 mm thick carbon/epoxy laminate is <500 J/cm^2." Nemes, et al. [21], using the Battelle data ([4] and [16]), computed the critical tensile stress at the spall plane to be 2.85 Kb for the 3-mm thick cross-ply laminated graphite/epoxy. From figure 11 of their paper, this equates approximately to a 100 J energy level. For the 6-mm diameter spot size and 30-ns pulse width, this would give a spall threshold intensity of 1.2 x 10^{10} W/cm^2 for the material at 1.06 μm wavelength.

Gilath and Eliezer [22] plot ablation pressure (Kb) versus sample thickness (mm) for three materials: Fe, Al, and CF/epoxy. The laminated carbon-fiber/epoxy material has the lowest damage threshold of the three materials tested. The data points for graphite/epoxy were picked from this graph [22]. The surface pressures were converted to equivalent laser intensities, using equation (4), and the results plotted in Figure 12 along with the one point from [21].

Kevlar/Epoxy

Tokheim, Erlich, Koboyaski, and Aidun [23] performed flyer-plate experiments on 7.62 mm thick laminated plates of Kevlar 49/ epoxy. They found a spall threshold of about 50 MPa for 1-μs pulses. As mentioned earlier, Kevlar/epoxy is partially transparent at laser radiation wavelengths. The energy coupling mechanisms for such materials are different than for the opaque materials [3] and direct comparison with the flyer-plate experiments may be difficult since we have no relationship between incident radiation and surface pressure for Kevlar/epoxy. Data presented by Walters and Clauer [14] is for samples that have an opaque coating to enhance energy

[3] Back surface values were measured in a quartz gage mounted on the back of the target and should be corrected for acoustic impedance mismatches.

coupling and increase the shocking ability of the available laser. A surface pressure of about 35 Kb reduces to about 9 Kb after traversing only 1.5 mm of material.[4] The measured shock speed was 3.0×10^5 cm/s in Kevlar/epoxy. These data are for a 30-ns pulse operating in a vacuum chamber and are reported in terms of surface pressure.

Carbon/PEEK

Reference [5] includes some experiments with 1.9 mm thick laminated carbon/PEEK thermoplastic composite material. The most striking results from this material was its relatively good residual strength after being laser-shocked.

[4] See footnote 3.

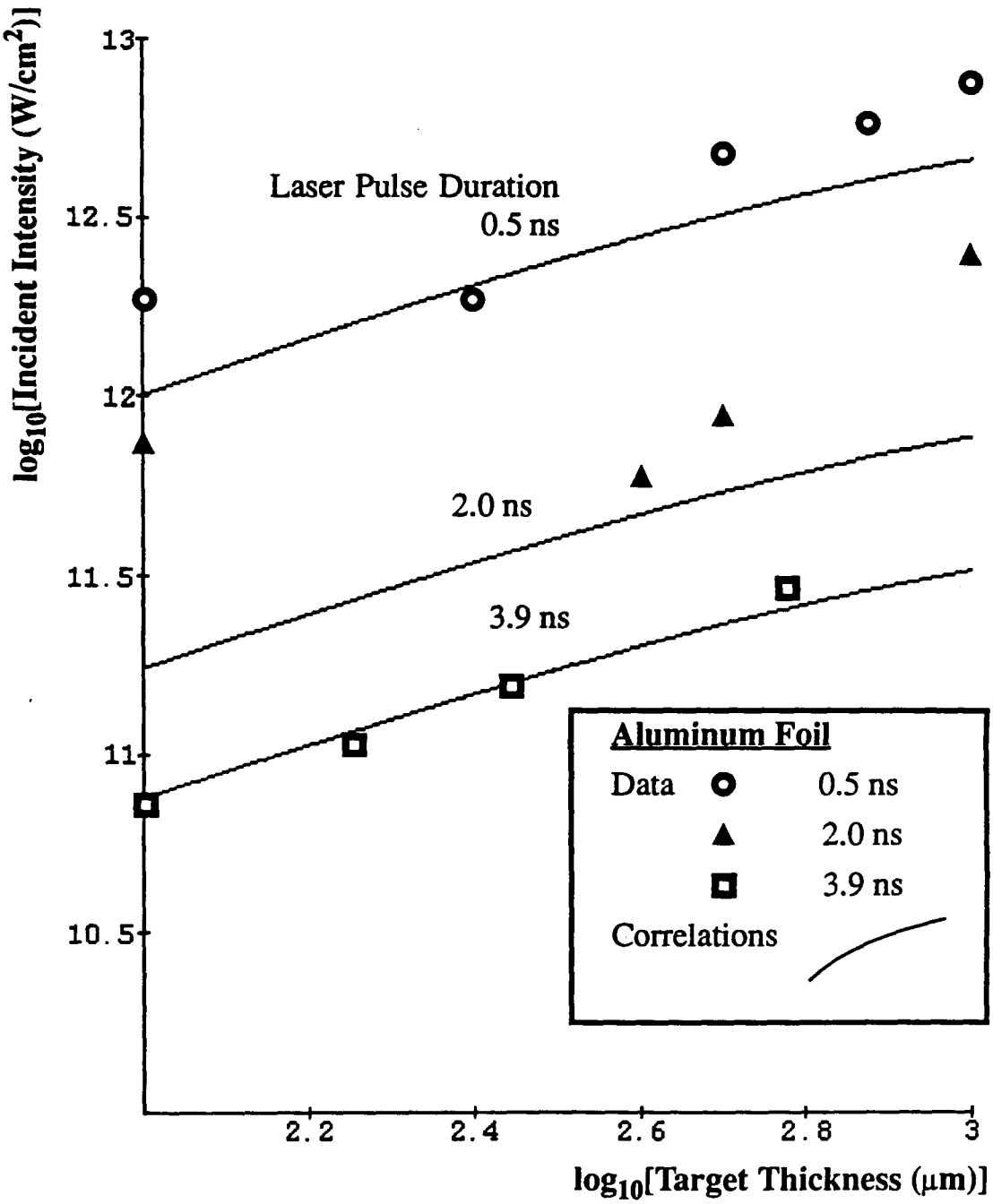

Figure 10. Spallation Thresholds for Aluminum Foil and Correlations with Developed Formulas (1.06 μm radiation at various pulse durations).

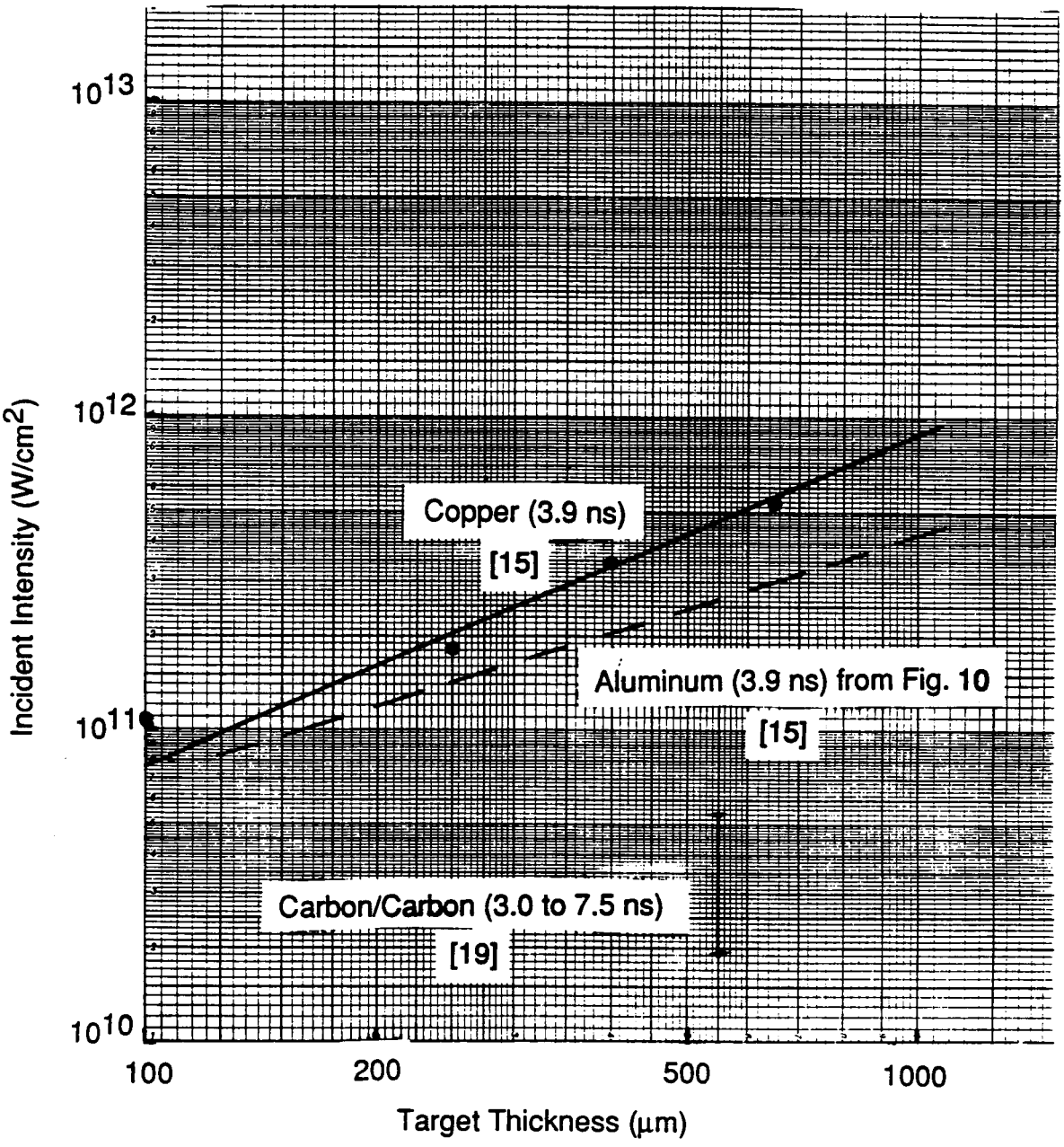

Figure 11: Comparison of Spalling Thresholds for Three Materials at Equal Pulse-Widths

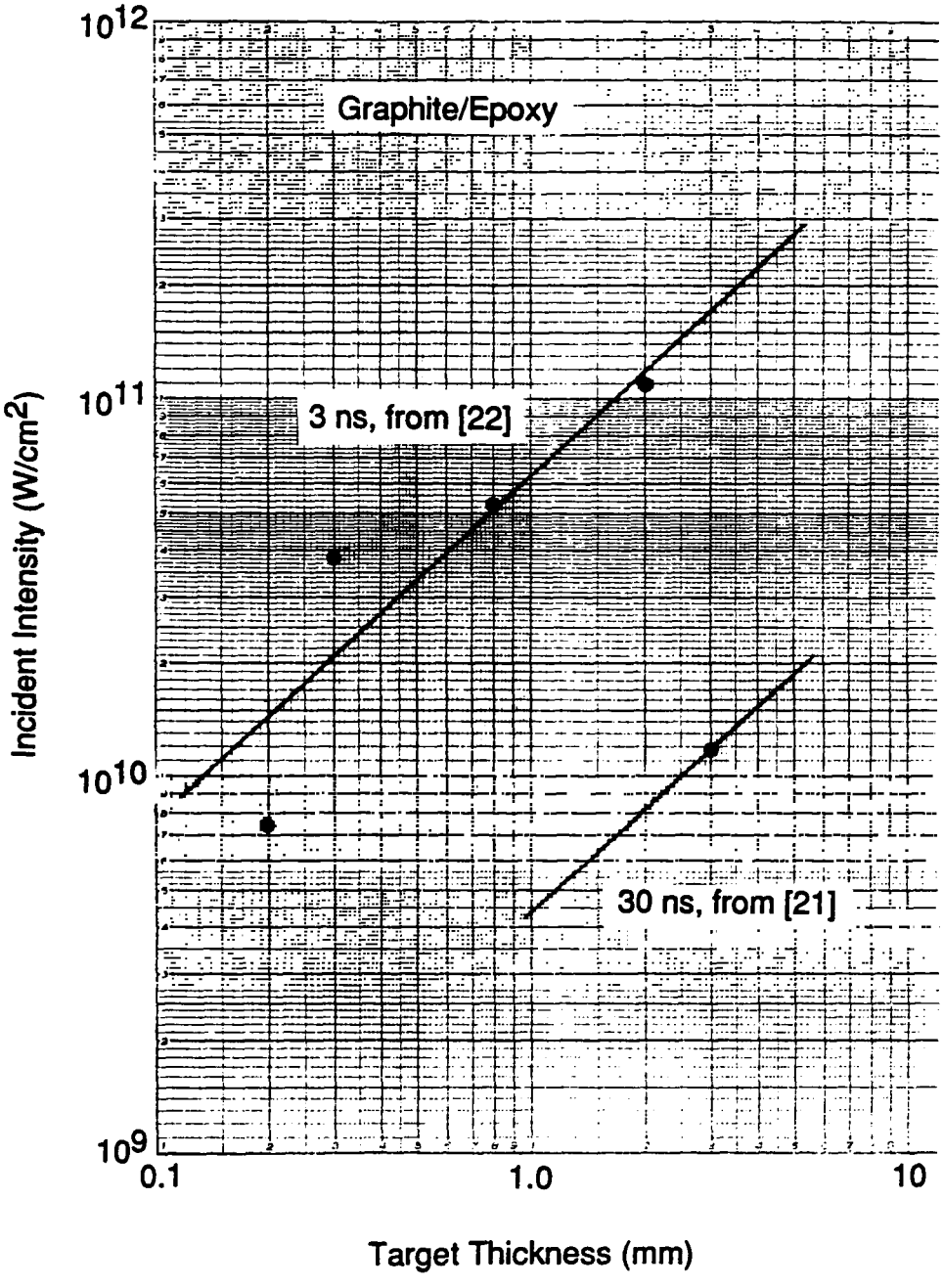

Figure 12: Spalling Thresholds for Graphite/ Epoxy (1.06 μm radiation)

References

1. M. S. Libeskind and T. E. Hess (NADC) and F. R. Stonesifer, C. A. Griffis, and C. I. Chang (NRL), "Effects of Laser Heating on Aircraft Structures (U)", Report No. NADC-88041-60, April 1988 (Confidential).

2. F. R. Stonesifer and G. W. Wissinger, "Survivability of GFRP Materials to Continuous Wave and Repetitively Pulsed Laser Irradiation", NRL Memorandum Report 6582, November 30, 1989.

3. J. A. Nemes and P. W. Randles, "Energy Deposition Phenomena in Partially Transparent Solids", J. Thermophysics, Vol. 3, No. 2, pp. 160-166, April 1989.

4. C. T. Walters, G. Newaz, J. L. Dulaney, and J. F. Scipione, "Shock Response in Advanced Materials (SRAM), Vol. I. Preliminary Investigation of Laser Effects", Battelle report BCD-G-0867-I, February, 1988.

5. C. T. Walters and G. Newaz, "Shock Response in Advanced Materials (SRAM)", Battelle Final Report BMI-G-1297, February, 1990.

6. A. H. Clauer, J. H. Holbrook, and B. P. Fairand, "Effects of Laser Induced Shock Waves on Metals", Chapter 38, *Shock Waves and High-Strain-Rate Phenomena in Metals, edited by M. A. Myers and L. E. Murr,* Plenum Pub. Corp., 1980.

7. J. A. McKay and P. M. Laufer, "Survey of Laser-Produced Pressure and Impulse Data", Physical Sciences Inc., report PSI-1012/TR-757, Sept. 1987.

8. G. A. Simons, "Momentum Transfer to a Surface When Irradiated by a High-Power Laser", AIAA Journal, 22, 1275 - 1280 (1984).

9. R. E. Beverly III and C. T. Walters, " Measurement of CO_2-laser-induced shock pressures above and below LSD-wave thresholds", J. Appl. Phys. 47 (8), August 1976.

10. A. N. Pirri, "Theory for momentum transfer to a surface with a high-power laser", Physics of Fluids, 16 (9), 1435-1440 September 1973.

11. Y. P. Raizer, "Propagation of discharges and maintenance of a dense plasma by electromagnetic fields", Sov. Phys. Uspekhi 15, 688-707 (1973);ibid., "Heating of a gas by a powerful light pulse", Sov. Phys. JETP 21, 1009-1017 (1965).

12. A. Edwards, N. Ferriter, J. A. Fleck,Jr., and A.M. Winslow, Lawrence Livermore Laboratory Report No. CRL-51489 1973 (unpublished, cited in [9]).

13. R. M. Christensen, *Mechanics of Composite Materials,* John Wiley and Sons, 1979, pp.225-273.

14. W. Herrmann, "Nonlinear Stress Waves in Metals", *Wave Propagation in Solids,* ASME, 1969, pp. 129-183.

15. S. Eliezer, I. Gilath, and T. Bar-Noy, "Laser-induced spall in metals: Experiment and simulation", J. Appl. Phys. 67 (2), 15 January 1990, pp. 715 - 724.

16. F. Cottet and M. Boustie, "Spall Measurements in Metallic Targets Using Shock Waves Induced by Short Duration Laser Pulses", *Shock Compression of Condensed Matter, edited by Schmidt, Johnson, and Davison,* Elsevier Science Publishers B. V., l990, pp. 425-428.

17. F. R. Tuler and B. M.Butcher, "A Criterion for the Time Dependence of Dynamic Fracture", The International Journal of Fracture Mechanics, Vol. 4, No. 4, 1968, p. 431.

18. F. Cottet and M. Boustie, "Spallation Studies in Aluminum Targets Using Shock Waves Induced by Laser Irradiation at Various Pulse Durations", J. Appl. Phys. 66 (9), 1 November 1989.

19. I. Gilath, S. Eliezer, and H. Weisshaus, "Damage in 2D Carbon-Carbon Composites by Short Pulsed Laser Induced Shock Waves", J. Reinforced Plastics and Composites, Vol. 8, May 1989.

20. C. T. Walters and A. H. Clauer, "Laser Shock Effects on Stressed Structural Materials", Battelle Report BCD-G-0463, July 21, 1986.

21. J. A. Nemes, P. W. Randles, and G. M. Newaz, "Structural Material Degradation Mechanisms Under Pulsed Laser Loading", AIAA Laser Effects and Target Response Conference. Montrerrey, CA, March 14-17, 1988.

22. I. Gilath and S. Eliezer, "Pulsed Laser Induced Spall, A New Method to Study Dynamic Properties", *1989 Advances in Plasticity, edited by Khan and Tokuda,* Pergamon Press, 1989.

23. R. E. Tokheim, D. C. Erlich, T. Kobayashi, and J. B. Aidun, "Characterization of Spall in Kevlar/Epoxy Composite", *Shock Waves in Condensed Matter, 1989, edited by S. C. Schmidt, J. N. Johnson, L. W. Davidson,* Elsevie Science Pub., B. V. Amsterdam (1990).